ThesisTitle

by

Daniel C. Cole

Other Degrees

A thesis submitted to the

Faculty of the Graduate School of the

University of Colorado in partial fulfillment

of the requirements for the degree of

Doctor of Philosophy

Physics Physics

2018

This thesis entitled:
ThesisTitle
written by Daniel C. Cole
has been approved for the Physics Physics

_____

Reader1

_____

Reader2

Date _____

The final copy of this thesis has been examined by the signatories, and we find that both the
content and the form meet acceptable presentation standards of scholarly work in the above
mentioned discipline.

Cole, Daniel C. (Ph.D., Physics)

ThesisTitle

Thesis directed by Dr. Scott A. Diddams

Nunc sed pede. Praesent vitae lectus. Praesent neque justo, vehicula eget, interdum id, facilisis et, nibh. Phasellus at purus et libero lacinia dictum. Fusce aliquet. Nulla eu ante placerat leo semper dictum. Mauris metus. Curabitur lobortis. Curabitur sollicitudin hendrerit nunc. Donec ultrices lacus id ipsum.

Acknowledgements

The work in this thesis would not have been possible...

- Acknowledgement line 1

- Acknowledgement line 2

Contents

Figures

Chapter 1

Introduction

1.1 Motivation

1.1.1 Seeing the invisible

Nulla malesuada porttitor diam. Donec felis erat, congue non, volutpat at, tincidunt tristique, libero. Vivamus viverra fermentum felis. Donec nonummy pellentesque ante. Phasellus adipiscing semper elit. Proin fermentum massa ac quam. Sed diam turpis, molestie vitae, placerat a, molestie nec, leo. Maecenas lacinia. Nam ipsum ligula, eleifend at, accumsan nec, suscipit a, ipsum. Morbi blandit ligula feugiat magna. Nunc eleifend consequat lorem. Sed lacinia nulla vitae enim. Pellentesque tincidunt purus vel magna. Integer non enim. Praesent euismod nunc eu purus. Donec bibendum quam in tellus. Nullam cursus pulvinar lectus. Donec et mi. Nam vulputate metus eu enim. Vestibulum pellentesque felis eu massa.

[1] Lorem ipsum dolor sit amet, consectetuer adipiscing elit. Ut purus elit, vestibulum ut, placerat ac, adipiscing vitae, felis. Curabitur dictum gravida mauris. Nam arcu libero, nonummy eget, consectetuer id, vulputate a, magna. Donec vehicula augue eu neque. Pellentesque habitant morbi tristique senectus et netus et malesuada fames ac turpis egestas. Mauris ut leo. Cras viverra metus rhoncus sem. Nulla et lectus vestibulum urna fringilla ultrices. Phasellus eu tellus sit amet tortor gravida placerat. Integer sapien est, iaculis in, pretium quis, viverra ac, nunc. Praesent eget sem vel leo ultrices bibendum. Aenean faucibus. Morbi dolor nulla, malesuada eu, pulvinar at, mollis ac, nulla. Curabitur auctor semper nulla. Donec varius orci eget risus. Duis nibh mi, congue

eu, accumsan eleifend, sagittis quis, diam. Duis eget orci sit amet orci dignissim rutrum.

Nam dui ligula, fringilla a, euismod sodales, sollicitudin vel, wisi. Morbi auctor lorem non justo. Nam lacus libero, pretium at, lobortis vitae, ultricies et, tellus. Donec aliquet, tortor sed accumsan bibendum, erat ligula aliquet magna, vitae ornare odio metus a mi. Morbi ac orci et nisl hendrerit mollis. Suspendisse ut massa. Cras nec ante. Pellentesque a nulla. Cum sociis natoque penatibus et magnis dis parturient montes, nascetur ridiculus mus. Aliquam tincidunt urna. Nulla ullamcorper vestibulum turpis. Pellentesque cursus luctus mauris.

Nulla malesuada porttitor diam. Donec felis erat, congue non, volutpat at, tincidunt tristique, libero. Vivamus viverra fermentum felis. Donec nonummy pellentesque ante. Phasellus adipiscing semper elit. Proin fermentum massa ac quam. Sed diam turpis, molestie vitae, placerat a, molestie nec, leo. Maecenas lacinia. Nam ipsum ligula, eleifend at, accumsan nec, suscipit a, ipsum. Morbi blandit ligula feugiat magna. Nunc eleifend consequat lorem. Sed lacinia nulla vitae enim. Pellentesque tincidunt purus vel magna. Integer non enim. Praesent euismod nunc eu purus. Donec bibendum quam in tellus. Nullam cursus pulvinar lectus. Donec et mi. Nam vulputate metus eu enim. Vestibulum pellentesque felis eu massa.

1.1.2   Femtosecond lasers

Nunc sed pede. Praesent vitae lectus. Praesent neque justo, vehicula eget, interdum id, facilisis et, nibh. Phasellus at purus et libero lacinia dictum. Fusce aliquet. Nulla eu ante placerat leo semper dictum. Mauris metus. Curabitur lobortis. Curabitur sollicitudin hendrerit nunc. Donec ultrices lacus id ipsum.

Chapter 2

EOM Combs

In this chapter, I discuss the generation of high-repetition-rate frequency combs through electro-optic modulation of a continuous-wave laser – so-called EOM combs [2]OTHERS. This scheme represents an alternative to parametric generation of HRR combs in Kerr resonators, and as the technology matures it will likely find a niche in the application space that leverages its long-term stability, lack of moving parts, and possibility for robust turn-key operation. First I present the operational principle and experimental results that represent the first generation of a coherent octave-spanning supercontinuum and detection of an active-modulation-based frequency comb's carrier-envelope offset frequency without an external optical reference. Then I provide a detailed discussion of the noise properties of the EOM comb, and I conclude with a proposal for future work.

2.1   Principle of operation

Generally, the EOM comb concept consists of passing a CW laser through cascaded phase and intensity modulators to generate a train of chirped pulses, and then propagating this pulse train through a dispersive medium to temporally compress the pulses to near their bandwidth-limited pulse duration. In a typical implementation, the pulses are generated with normal (in contrast with anomalous) chirp – the carrier frequency increases over the pulse duration. This allows compression via propagation in standard, anomalously dispersive optical fiber. In this case an expression for the electric field before temporal compression results from the product of the field $E_o e^{-i\omega_c t}$ with the intensity modulation $\frac{1}{2}\left\{\exp\left[i\frac{\pi}{4}(1+\sin\omega_r t)\right] + \exp\left[-i\frac{\pi}{4}(1+\sin\omega_r t)\right]\right\}$ and

the phase modulation $\exp\left[i\beta_m \sin\omega_r t\right]$. Here representing the intensity modulation as the sum of exponential terms (instead of using the equivalent representation with $\cos\omega_r t$) is indicative of the fact that the intensity modulation arises from simultaneous phase modulation in two paths. The resulting electric field (up to a constant overall phase shift relative to the previous expressions) is:

$$E = E_o \cos\left(\frac{\pi}{2}\sin^2\frac{\omega_r t}{2}\right) e^{i\omega_c t - i\beta_m \cos\omega_r t}. \tag{2.1}$$

This can be understood as the product of a time-varying real amplitude $a(t) = E_o \cos\left(\frac{\pi}{2}\sin^2\frac{\omega_r t}{2}\right)$ and a phase factor from which the instantaneous carrier frequency $\omega(t) = \omega_c + \omega_r\beta_m \sin\omega_r t$ can be calculated. The carrier frequency $\omega(t)$ is increasing when the amplitude $a(t)$ is at its maximum, corresponding to normal chirp on the pulses.

2.2 Detection of the carrier-envelope offset frequency of an EOM comb

Here I describe generation of an EOM comb with 10 GHz repetition rate and subsequent measurement of its carrier-envelope offset frequency. The experimental setup is depicted in Fig. 1a. The basic experimental scheme consists of the following steps: 1. Initial generation and temporal compression of the EOM comb pulse train; 2. Spectral broadening and temporal re-compression; 3. Noise reduction using a Fabry-Perot filter cavity; and 4. Octave-spanning supercontinuum generation and detection of the carrier-envelope offset frequency. The results described below represent the first time a frequency comb based on active modulation of a CW laser has been self-referenced. Key to the success of this approach is the implementation of nonlinear spectral broadening in two stages, which allows the second stage to be seeded with $\sim$100 fs pulses for coherent supercontinuum generation, and also the noise reduction stage, described below.

To generate the initial train of chirped pulses, a telecom-band continuous-wave laser is passed through cascaded phase and intensity modulators driven with a 10 GHz microwave signal. The intensity modulator is biased at the 50 % transmission point and driven with an RF amplitude of $V_\pi/2$. The phase modulator is driven with modulation depth of $\sim 31\pi/4 \sim 24.3$ rad. The relative

phase between the modulators is set such that the phase applied by the phase modulator is at a minimum when the transmission of the intensity modulator is highest; this yields a train of up-chirped pulses. Simulated temporal intensity and instantaneous carrier-frequency profiles are shown in Fig. 1b, and a simulated optical spectrum is overlaid on an experimental measurement in Fig. 1c.
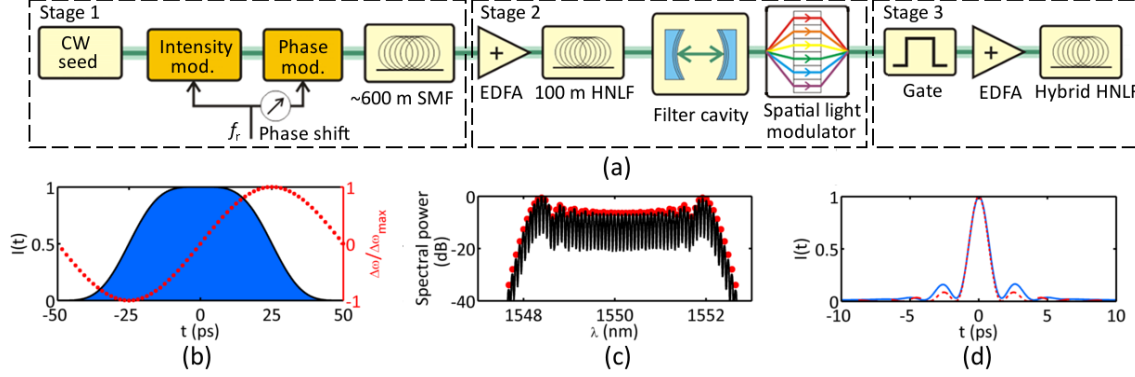

Figure 2.1: **BFCaption.** Caption

Next, the chirped pulse train is propagated through 600 m of anomalously-dispersive SMF. The length of SMF that is appropriate for pulse compression depends on the bandwidth of the optical pulses to be compressed; equivalently it depends on both the phase-modulation depth and the repetition rate of the pulse train. This temporal compression reduces the duration of the optical pulses from $\sim$50 ps to $\sim$ 1.5 ps. A simulation of the resulting intensity profile is presented in Fig. 1d.

The compressed pulses are amplified to 400 mW average power in an erbium-doped fiber amplifier and launched into 100 m of HNLF. This section of HNLF has chromatic dispersion that is small and normal; this is carefully chosen to chirp the pulses via self-phase modulation while avoiding soliton-fission dynamics. The result is a train of chirped $\sim$1.5 ps pulses exiting the fiber. In Fig. 2a we present the measured optical spectrum of this pulse train, as well as results of a numerical simulation of the spectral broadening in the 100 m of normally-dispersive HNLF. These simulations are conducted using the nonlinear Schrodinger equation (NLSE) including third order dispersion, taking as initial conditions the calculated intensity profile of the EOM comb pulses shown in Fig.

1d. The dispersion values for the HNLF used in the simulation are $D = -0.04$ ps/nm·km and $D' = 0.003$ ps/nm²·km, close to the values specified by the manufacturer. The simulation method is described in detail in App. **??**.

After propagation through the first section of HNLF, the pulses are passed through a high-finesse Fabry-Perot cavity for suppression of optical frequency fluctuations as discussed below. Then the pulses are temporally compressed again, this time using a spatial light modulator (SLM) [3]; narrow spectral regions are resolved using a grating and passed through individually controlled delaying elements, then recombined. The SLM applies 2nd, 3rd, and 4th order chromatic dispersion, which simulations indicate is sufficient to compress the pulses to ∼130 fs, nearly the transform limit. This is shown in Fig. 2b. It would also be possible to compress the pulses via propagation in an appropriate length of SMF, although this is less convenient than the compression of the initial EOM comb pulse train in SMF described above due to stronger fluctuations in the output over time associated with the nonlinear origin of the chirp. Figs. 2b and 2c present the output intensity profile and the evolution of the intensity profile, respectively, in simulated compression in SMF. Because the pulses are broadband, temporally short, and reasonably high energy, these simulations are performed including the full dispersion profile of SMF and the Kerr nonlinearity.

The temporally compressed ∼130 fs pulses are then passed through a Mach-Zehnder modulator functioning as an electro-optic gate for repetition-rate downsampling (see Chapter 3). The gate selectively transmits every fourth pulse, reducing the repetition rate of the pulse train to 2.5 GHz. This facilitates coherent supercontinuum generation in a second stage of spectral broadening by increasing the pulse energy that can be achieved at a given average power. Note that this step is convenient but not strictly necessary, as shown in Ref. [4].

The downsampled 2.5 GHz pulse train is amplified to an average power of 1.4 W, resulting in a train of ∼ 0.56 nJ pulses. This pulse train is propagated through 8 m of hybrid HNLF, yielding the spectrum shown in Fig. 2d. This hybrid HNLF consists of two segments with different dispersion profiles, with each segment serving a different purpose. The first segment is 30 cm long and highly dispersive ($D = 6$ ps/nm·km), and generates a dispersive wave centered at 1090 nm. The second

segment is 7.7 m long and has lower dispersion ($D = 1.5$ ps/nm·km), and generates a Raman-self-frequency-shifted soliton centered near 2150 nm. The effect of each of these fibers on the output spectrum can be understood by investigating propagation in each section separately. To do this we use the LaserFOAM program [5], which employs the generalized NLSE including Raman scattering, self-steepening, and 2nd- through 4th-order dispersion. The simulations are run independently, and both take as their initial conditions 170 fs Gaussian pulses with 350 pJ energy, close to the energy coupled into the HNLF after accounting for losses. The results of these simulations are plotted in Fig. 2d.
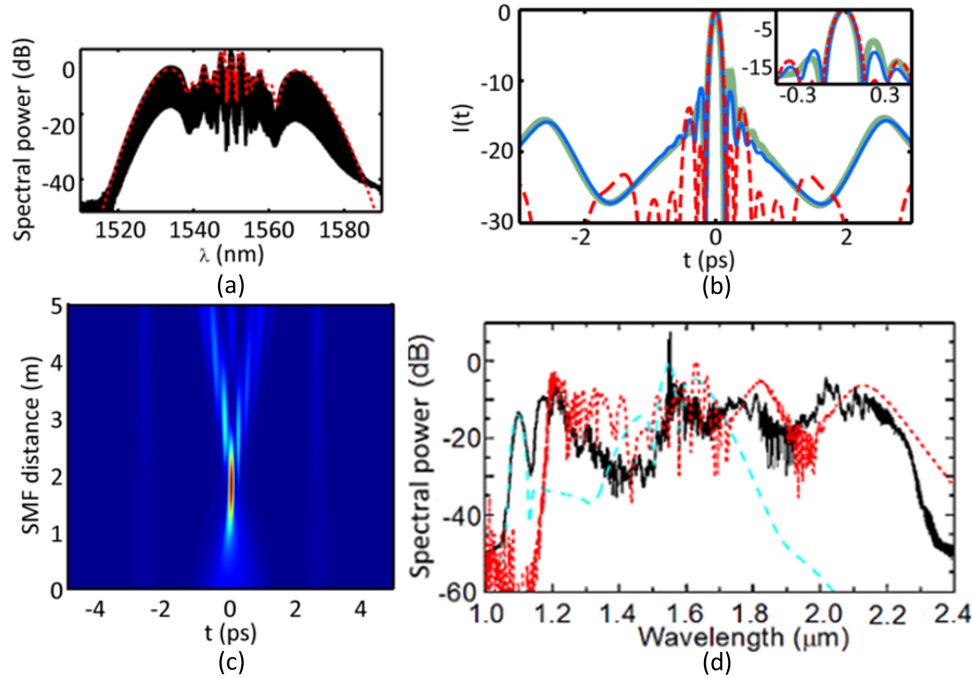
Figure 2.2: **BFCaption.** Caption

The supercontinuum generated in the hybrid HNLF is coherent and suitable for $f - 2f$ self-referencing. To detect the carrier-envelope offset frequency of the EOM comb, we pass the pulse train through an interferometer consisting of a dichroic mirror, a delay stage in one path, and a 10 mm sample of periodically-poled lithium niobate that generates the second harmonic of supercontinuum light at 2140 nm. The dichroic mirror and delay stage enable adjustment of the relative timing between the native 1070 nm and doubled 2140 nm components of the supercontinuum so that they are

temporally coincident. An optical band-pass filter centered at 1070 nm selects the supercontinuum components required for self-referencing, shown in Fig. 3a, and impinging the filtered light on a photodetector reveals the carrier-envelope offset frequency of the EOM comb, shown in Fig. 3b. Note that downsampling introduces an ambiguity in the offset frequency due to the increased density of comb modes in the downsampled pulse train; this ambiguity can be removed by measuring the change in measured offset frequency with a change in $f_r = \omega_m/2\pi$ provided by the synthesizer driving the modulators.
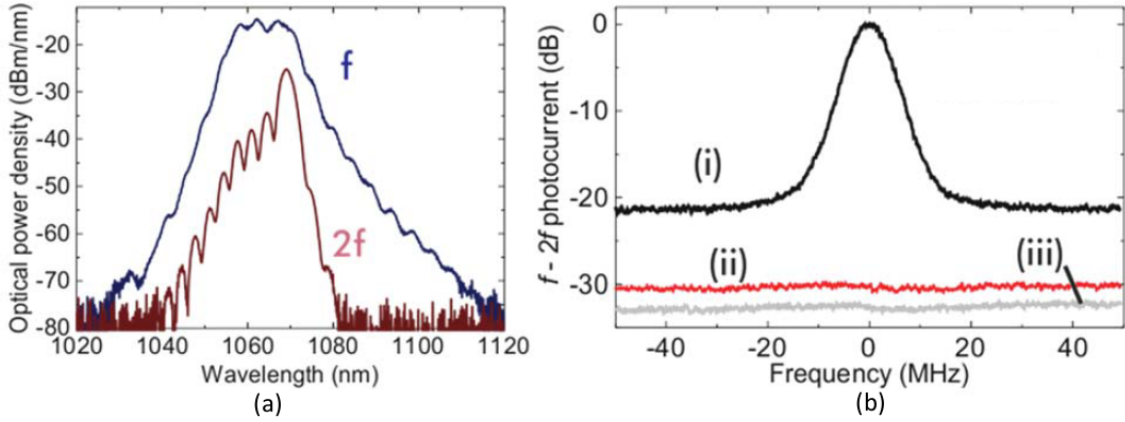
Figure 2.3: **BFCaption.** Caption

2.3   Noise in EOM Combs

An important difference between the EOM comb scheme and other approaches for generation of frequency combs is that the repetition rate is derived directly from a microwave source and is directly multiplied by a factor N to yield the optical frequency of mode number N from the pump (where $N = 0$). Therefore, the contribution to the optical frequency noise of mode number N from the microwave source scales with the mode number N, and the contribution to the power spectrum of frequency noise scales as N^2. This presents a challenge in the generation of coherent supercontinuum light, where the modes relevant for $f - 2f$ self-referencing are far separated from the pump laser. The factor by which the noise on the modulation tone f_r is multiplied to determine its contribution to the noise on the measured carrier-envelope offset frequency is the ratio between the comb's carrier

frequency (the frequency of the seed laser) and the repetition rate: $N = f_c/f_r$ =19340 for the 10 GHz comb discussed above (where f_c =193.4 THz for a 1550 nm pump laser). This contribution is shown in Fig. 3a, along with the contribution from the CW seed laser. The noise on f_r results from technical noise on the synthesizer tone at low Fourier frequencies and approaches a white Johnson-Nyquist (thermal) phase-noise floor of -177 dBm/Hz at high Fourier frequencies. As discussed in Ref. [4], unmitigated multiplication of this noise floor by the factor N =19340 leads to a supercontinuum with optical frequency fluctuations that are large enough to prevent detection and measurement of f_0.

To address this problem and enable $f - 2f$ self-referencing of our comb, we pass the comb through a Fabry-Perot filter cavity whose free-spectral range is actively stabilized to the comb's mode spacing. The filter cavity's Lorentzian transfer function reduces the optical frequency fluctuations of the comb modes at high frequency – these fluctuations are averaged over the photon lifetime of the cavity. This enables generation of a supercontinuum with resolvable modes that is suitable for $f - 2f$ self-referencing and measurement of f_0.

The filter cavity used for this 10 GHz comb has a 7.5 MHz linewidth; equivalently, it has finesse of $F \sim$1333. The effect of passing the comb through the cavity is demonstrated concretely in Fig. 3b, where we compare the lineshape of a heterodyne beat between the supercontinuum and a CW laser with 1319 nm wavelength with and without the filter cavity in place. The signal-to-noise ratios for the beat with and without the filter cavity are 40 dB and 17 dB, respectively.
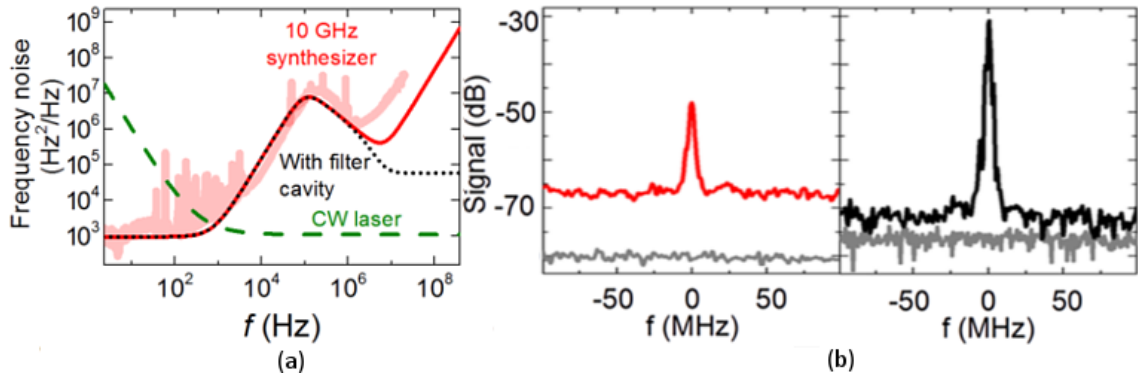

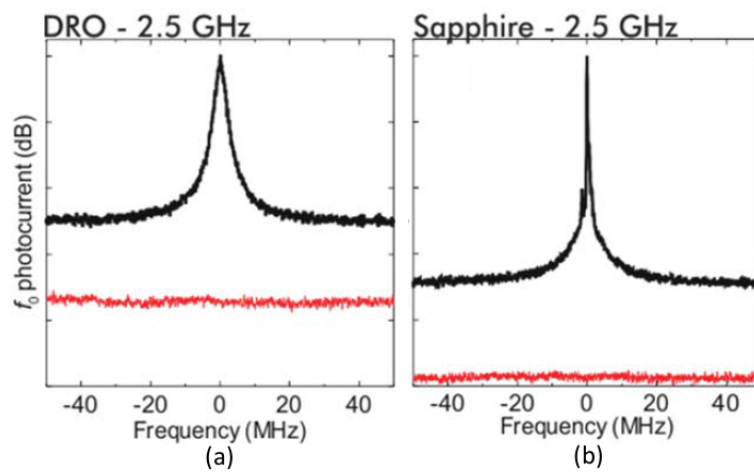Figure 2.4: **BFCaption.** Caption

Figure 2.5: **BFCaption.** Caption

Chapter 3

Pulse Picking

This chapter presents a discussion of a technique for repetition-rate reduction of optical pulse trains. While high pulse train repetition rates are appealing for some applications, they are not always appropriate. For example, spectral resolution is sacrificed in a comb with a large mode spacing, and a high repetition rate makes nonlinear optics less efficient at a given average power. This can present a barrier to the achievement of octave-spanning spectra for $f - 2f$ self-referencing. On the other hand, the size of the comb package sets the scale for round-trip time, meaning that low-SWAP combs generally have inherently high repetition rate. Therefore, to increase the flexibility of low-SWAP and high-repetition-rate comb systems in applications, a method for reducing the repetition rate of a pulse train will be useful.

Here I present an investigation of a method for repetition-rate reduction, or downsampling, in which an electro-optic gate realized by an RF-driven Mach-Zehnder interferometer periodically transmits an incoming pulse at a frequency lower than the input repetition rate. The basic principle is illustrated in Fig. 3.1. Downsampling via pulse gating, also referred to as "pulse picking" in the literature, has been used extensively in the context of high-field, phase-sensitive ultrafast optics for the generation of energetic, carrier-envelope-phase-stabilized ultrashort pulses[6, 7]. In this application, a comb with initial repetition rate in the 100 MHz range that has already been stabilized is pulse-picked to a repetition rate on the order of 1-100 kilohertz. Concerns in this application center around control and preservation of the carrier-envelope phase in the pulse-picking and amplification process[8, 9]. In this paper we consider downsampling within the context of optical metrology with

frequency combs, and we are concerned with downsampling's effect on the optical phase noise, the pulse-to-pulse energy fluctuations, and the carrier-envelope offset frequency. In particular, it is important that the downsampled pulse train is suitable for $f - 2f$ self-referencing.

Sec.3.1 presents a proof-of-principle experiment in which a 250 MHz pulse train is downsampled to 25 MHz, and then spectrally broadened and self-referenced. A mathematical model of downsampling is presented in Sec. 3.2, and this model informs the discussion of downsampling's effect on the pulse train's noise properties presented in Sec. 3.3 and Sec. 3.4. In Sec. 3.4.1 I discuss some practical considerations in application of the technique, including the effect of imperfections in the gating process such as incomplete extinction of rejected pulses.
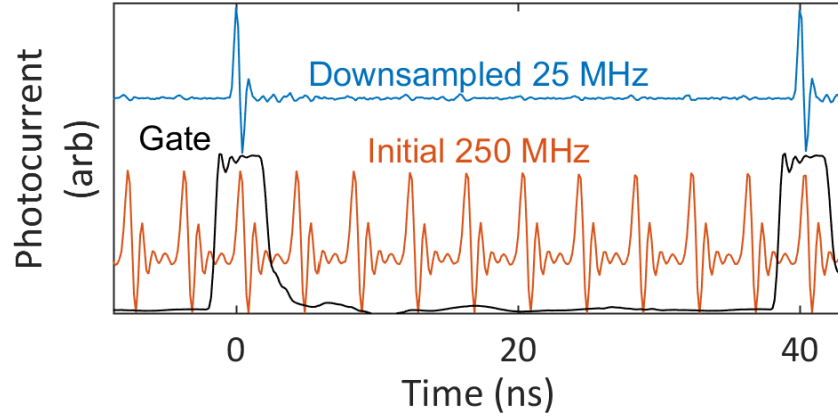

Figure 3.1: **Photodetected optical pulse trains illustrating downsampling.** Orange: Photodetected 250 MHz pulse train. Blue: The same, photodetected after downsampling to 25 MHz. Black: Oscilloscope trace showing the voltage sent to the RF port of a Mach-Zehnder amplitude modulator to selectively transmit a subset of the incoming pulses.

3.1   Proof-of-Concept Experiment

The application of downsampling to the detection of the carrier-envelope offset frequency of a 250 MHz comb is shown in Fig. 3.2. Our pulse gating scheme, shown in Fig. 3.2a, employs a Mach-Zehnder (MZ) electro-optic intensity modulator driven by 25 MHz rectangular electronic gating pulses with 80 ps transitions and 3.5 ns duration. The electronic pulse generator and the repetition rate of the input 250 MHz comb are both referenced to a hydrogen maser to maintain

synchronization. The DC bias of the EOM is set for maximum extinction outside the electronic gate, whose amplitude is matched to V_π of the EOM. This downsampling scheme results in a stable 25 MHz optical pulse train with >12 dB contrast (Fig. 3.1b). This extinction ratio is sufficient for this proof-of-concept but could be improved by cascading modulators with higher extinction ratios. The average power of the 250 MHz pulse train is reduced from 30 mW to 400 μW by the pulse gating process and the insertion loss of the optical components. We amplify the pulse train to 35 mW by use of a normal-dispersion erbium-doped fiber amplifier, which provides some spectral broadening and temporal pulse compression 22. An octave-spanning supercontinuum is obtained by launching the amplified, <100 fs, ~1 nJ pulses into 20 cm of highly nonlinear fiber (HNLF)[10]; the resulting spectrum is shown in Fig. 3.2c. For comparison, we also present the supercontinuum generated by the 250 MHz comb with the EOM set for constant maximum transmission under otherwise identical conditions. The 250 MHz comb is amplified by the same EDFA to an average power of 85 mW, corresponding to 340 pJ pulse energy, before it enters the HNLF.

To detect f_0, the octave-spanning supercontinuum shown in Fig. 3.2b is sent into a free-space $f - 2f$ interferometer consisting of a half-wave plate and a periodically poled lithium niobate (PPLN) crystal quasi-phase-matched for second-harmonic generation at 1980 nm. The generated 990 nm light is shown in 3.2b. A 10 nm band-pass filter at 990 nm selects this second harmonic and the co-linear supercontinuum at 990 nm, which are then photodetected to observe f_0 with 30 dB signal-to-noise ratio, shown in Fig. 3.2c. Fig. 3.2d shows a 2000 s record of f_0 for the downsampled comb.

3.2   Mathematical model for downsampling

While Fig. 3.2 presents an absolute frequency measurement of f_0 enabled by downsampling, it does not demonstrate the deterministic connection between the input and downsampled combs that is essential for applications. To understand this relationship, I present first a simple model of downsampling, and then experimental tests of its conclusions.

The downsampled pulse train's electric field is modeled as the product of the incoming comb's
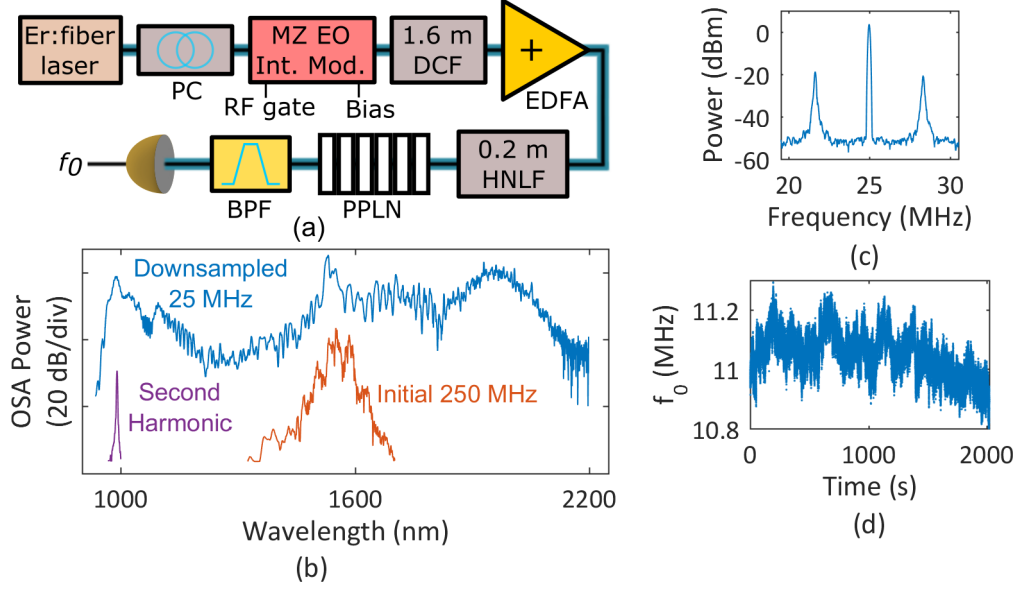
Figure 3.2: **Demonstration of downsampling for f_0 detection.** (a) Schematic for downsampling a 250 MHz Er:fiber comb and detecting the offset frequency of the resulting 25 MHz pulse train. PC – polarization controller. DCF – dispersion-compensating fiber. EDFA – erbium-doped fiber amplifier. HNLF – highly nonlinear fiber. PPLN – periodically-poled lithium niobate. BPF – (optical) band-pass filter.(b) Octave-spanning supercontinuum generated by downsampling (top, blue), second harmonic generated for f0 detection (purple), and for comparison the supercontinuum generated by the same apparatus without downsampling (orange). (c) Detected repetition rate and f_0 beat at 100 kHz RBW; signal-to-noise ratio of f_0 is 30 dB. e) Counted frequency of the detected free-running offset beat. Data is taken for 2000 s at 10 ms gate time. The offset frequency of the 250 MHz commercial comb was adjusted between measurements shown in Figs. 3.2c and 3.2d to simplify electronic processing.

field and a time-varying amplitude modulation. For an incoming optical frequency comb with repetition rate f_r, complex single-pulse field $A(t)$ that is localized near $t = 0$, and pulse-to-pulse carrier-envelope phase shift ϕ, pulse gating by a train of rectangular pulses of length t_g and arrival rate f_g yields a downsampled comb with field

$$a(t) = \left[\Sigma_n A(t - n/f_r)e^{in\phi}\right] \times \left[\Sigma_m \text{Rect}\left((t - m/f_g)/t_g\right)\right] \tag{3.1}$$

where $\text{Rect}(x)$ is the rectangle function, taking the value 1 for $-1/2 \leq x \leq 1/2$ and 0 elsewhere. Indices n and m count the pulse number of the incoming pulse train and the electronic gate respectively. The optical spectrum of the downsampled pulse train $a(t)$, calculated via the convolution theorem for the Fourier transform, is:

$$\mathcal{F}\{a\}(f) \sim 4\pi f_r \Sigma_{nm} \frac{1}{m} \mathcal{F}\{A\}(f_0 + nf_r) \times \sin(\pi m t_g f_g)\delta(f - f_0 - nf_r - mf_g) \tag{3.2}$$

where $f_0 = (f_r \cdot \phi/2\pi$ is the carrier-envelope offset frequency of the incoming comb and δ is the Dirac delta function. The downsampled pulse train has spectral content at optical modes $f_0 + nf_r$, as well as at intensity modulation sidebands whose frequency offsets mf_g are harmonics of the gating frequency. To avoid the generation of unwanted modulations, pulse gating at an integer sub-harmonic of the incoming repetition rate, $f_g = f_r/N$, is essential. In this case superposition of the intensity modulation components created by pulse gating results in a downsampled frequency comb with a single mode spacing. Moreover, this model predicts that the offset frequency is preserved up to a reduction modulo the comb's new repetition rate.

Notably, for pulse gating at a sub-harmonic of the input comb's repetition rate, timing jitter of the electronic gate that is less than its duration does not contribute to noise on the downsampled comb. By modelling jitter as gate-to-gate arrival-time delays Δt_m, it can be shown that the down-sampled comb's amplitude $a(t)$ and spectrum $F\{a\}(f)$ do not deviate from Eqn. 3.1 provided that: 1) The jitter is a sufficiently small $|\Delta t_m| < t_g/2$, i.e., that the optical and electronic pulses are always substantially overlapped, and 2) That the optical pulses are substantially shorter than the electrical pulses, which is true for most systems. Thus, in general we expect that the carrier-envelope offset frequency of the incoming comb is preserved by downsampling even with jitter on the gate signal.

3.3   Experimental investigation of the effect of downsampling on the pulse train's noise properties

We supplement the mathematical model presented above with an experimental investigation of the effects of downsampling on the noise properties of the pulse train. First we consider the effects of technical limitations to ideal downsampling, and then we discuss fundamental effects associated with aliasing of high-Fourier-frequency optical noise and shot noise.

We measure the phase-noise spectrum of the downsampled comb's repetition rate at different points in our apparatus, as shown in Fig. 3.3a. We also plot the phase noise of the 250 MHz comb, which has been shifted by $-10\log_{10}(N^2) = -20$ dB to facilitate comparison[11], and the phase noise of the electronic gate. The downsampled frequency comb's phase-noise spectrum matches that of the

250 MHz comb except for a small increase at ~3 kHz, likely corresponding to the corner in the gate

generator's phase noise at the same frequency. The phase noise of the high- and low-frequency ends

of the supercontinuum similarly matches the 250 MHz comb below 1 kHz. The higher phase noise in

the supercontinuum beyond 1 kHz is likely due to noise generation processes in the HNLF, such as

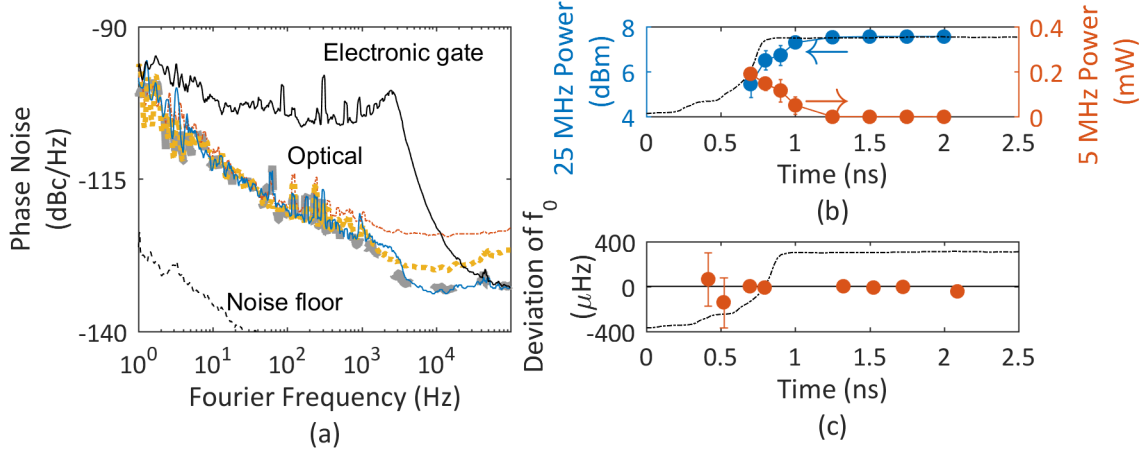the conversion of amplitude fluctuations on input pulses to timing jitter in the supercontinuum[12].

Figure 3.3: **Experimental investigation of noise introduced by downsampling.** (a) Measured repetition-rate phase noise of spectral components of the supercontinuum, selected by a 990±5 nm band-pass filter (dot-dashed orange), 1650 nm long pass filter (dotted yellow), and the entire downsampled 25 MHz frequency comb measured immediately before the EDFA (solid blue), the 250 MHz comb (large-dashed gray, shifted by $20\log(1/10) = -20$ dB. Also shown is the phase noise of the electronic gate generator (top, solid black). (b) Amplitude of the downsampled pulse-train modulation due to 250 ps jitter at 5 MHz rate. The position of a data point on the x-axis indicates its mean position within the gate, shown in dashed black. Measurement uncertainties arise due to a latency between the optical trigger and the start of the electronic gating signal which varies on the order of 50 ps. (c) Deviation of the carrier-envelope offset frequency of the downsampled comb from the 250 MHz comb's offset frequency as a function of the alignment of optical pulses within the gate.

The timing jitter of our gating pulse train is between 5 ps (obtained by integrating the phase

noise plotted in Fig. 3.3 to 100 kHz) and 10 ps (extrapolating constant phase noise to the 12.5

MHz Nyquist frequency and integrating). These jitter values are small relative to the 4 ns repetition

period of the incoming optical pulse train. As the repetition rate of the incoming optical pulse train

increases to >10 GHz, the gate duration must correspondingly decrease for single-pulse gating, and

timing jitter on the gate may become a significant fraction of the gate duration. To explore the

effects of timing jitter larger than our pulse generator's inherent 5 to 10 ps, we impose excess jitter

on the gating signal. We modulate the relative timing between the gating signal and the incoming optical pulse train at a frequency of 5 MHz with an amplitude of 250 ps. The effect of this jitter is manifest in the microwave power of the gated comb as 5 MHz intensity-modulation sidebands whose amplitude depends on the position of the optical pulses within the gate, as shown in Fig. 3.3b. Pulses with a mean position within 250 ps of the gate edge are substantially modulated by the 5 MHz gate-delay signal. This agrees with the prediction of a sharp threshold on the acceptable level of timing jitter on the gate.

It is essential to establish that the comb's carrier-envelope offset frequency is preserved in the downsampling process. To do this, we perform a frequency comparison of the 25 MHz downsampled comb and a separate output of the 250 MHz comb. This 250 MHz output is intensity modulated so that a measurement of the nonzero optical heterodyne beat frequency between an intensity modulation sideband and a pulse-gating sideband of the downsampled comb reveals the relative frequency offset of the two combs. Figure 3.3c shows the null frequency shift between the 25 MHz and 250 MHz combs, which we have characterized for different alignments of the optical pulse within the gate. At the level of several microhertz, better than 10^{-18} relative to the 200 THz optical carrier frequency, we observe no frequency shift between the 250 MHz comb and the downsampled 25 MHz comb when the gate is properly aligned. This confirms the utility of downsampling for measurement of a high-repetition-rate comb's offset frequency for subsequent use of the comb in, for example, a spectroscopy experiment requiring high power per comb mode and high frequency precision.

3.4   Effects of ideal downsampling on a pulse train's noise properties

In addition to the conversion of electronic technical noise to optical noise on the downsampled pulse train, there exists a further mechanism by which downsampling can change the measured amplitude noise properties of the pulse train. Even ideal downsampling, free of electronic noise, leads to an increase in the measured power spectral density (PSD) of optical pulse energy fluctuations (PEF) when technical pulse energy noise is present. This is due to aliasing of components of the PSD of pulse energy fluctuations at frequencies above the Nyquist frequency, $f_r/2$, when the

Nyquist frequency is reduced by downsampling. Assuming random fluctuations from pulse to pulse, downsampling does not change the RMS fractional pulse energy fluctuation σ_{PEF}, whose square is equal to the frequency integral of the PSD of pulse energy fluctuations $S_{PEF}(f)$:

$$\sigma_{PEF}^2 = \int_0^{f_r/2} df\, S_{PEF}(f). \tag{3.3}$$

—

Because the Nyquist frequency $f_r/2$ defines the upper limit for integration of S_{PEF}, in order for σ_{PEF} to be preserved $S_{PEF}(f)$ must increase when the Nyquist frequency is reduced. For example, in the simple case of white technical noise on the pulse energies with density S_o, we have

$$\sigma_{PEF}^2 = \int_0^{f_r/2} df\, S_o = \int_0^{f_r/2N} df\, S' \tag{3.4}$$

which shows that downsampling must increase the measured PSD of white technical noise from S_o to $S' = NS_o$, assuming there are no spectral correlations. However, this simple multiplicative increase is restricted to the case of white technical noise. In general, the PSD of pulse energy fluctuations of the new pulse train is determined from the original PSD through the usual method of modeling aliasing of a signal: a new Fourier frequency for each component of the original PSD is obtained by reducing the original Fourier frequency by a multiple of $-f_r/N$ so that it lies between $-fr/2N$ and $f_r/2N$ and taking its absolute value. The new PSD is then determined by taking the quadrature sum of the PSD components at the same aliased Fourier frequency. This phenomenon is derived mathematically and demonstrated experimentally in Ref. [8], where the analysis of carrier-envelope phase noise applies equally well to pulse energy fluctuations.

In contrast with the increase in the PSD of pulse energy fluctuations arising from coincidence of the optical pulse with the edge of the electrical gate, which increases σ_{PEF}, the aliasing mechanism described above preserves σ_{PEF}. An important consequence of this is that while technical noise can lead to supercontinuum decoherence in external nonlinear spectral broadening, aliasing does not, because it is σ_{PEF} which determines the degree of supercontinuum decoherence. Thus the aliasing mechanism impedes $f - 2f$ self-referencing only by reducing the available signal-to-noise ratio of an

f_0 signal in a straightforward linear fashion.

In practice, the relevance of the aliasing of the PSD of pulse energy fluctuations is determined by the presence of technical noise on the pulse energies at high Fourier frequency $f > f_r/2N$. For sufficiently small downsampling factors (e.g. $f_r/2N \leq\sim 50MHz$) and depending on the comb source, it is possible that the only source of intensity noise at frequencies above $f_r/2N$ is shot noise. Shot noise results in a maximal (shot-noise-limited) signal-to-noise (SNR) ratio of an optical heterodyne beat with a local oscillator laser which is reduced by N^2 (in electrical power units) as the average power of the pulse train is reduced by downsampling by a factor of N. In contrast, in the case of detection of a carrier-envelope-offset beat with fixed optical detection bandwidth, the shot-noise-limited SNR is preserved in downsampling. One way to understand these results is to model the shot noise at a given Fourier frequency as the incoherent sum of optical heterodyne beats between each optical comb mode and the uncorrelated vacuum fluctuations at the appropriate optical frequency25,26, and to take into account the fact that during downsampling the optical power of each comb mode is reduced by N^2, with the first factor of N coming from reduction of the total optical power and the second factor of N due to the increase in the spectral density of comb modes.

We experimentally investigate the impact of downsampling on the PSD of pulse energy fluctuations by measuring noise on three photodetected optical signals: a shot-noise-limited telecom-band CW laser, a 10 GHz pulse train generated by passing this laser through cascaded optical phase and intensity modulators (see Chapter **??**, [13]) and then a low-noise EDFA, and this pulse train after downsampling by a factor of four to 2.5 GHz repetition rate with no additional amplification after downsampling. Shown in Figure 3.4 are curves for each signal of the fluctuations $\sqrt{S_I(f = 50\,\mathrm{MHz})}$ in the detected photocurrent at a Fourier frequency of 50 MHz versus the total time-averaged detected photocurrent $\langle I \rangle$ from the optical signal. To measure the scaling of noise with optical power, these curves are generated by beginning with an optical signal which yields more than 800 μA of detected photocurrent and attenuating this signal before photodetection. The data indicate that both the pulse-generation process and the downsampling process contribute some amount of technical

noise at 50 MHz Fourier frequency to the photocurrent, because the measured curves are well-modeled by a quadrature sum of a shot-noise contribution and a technical noise contribution. The contributions of these two types of noise can be determined because they scale differently with the photodetected power: shot noise obeys the relationship $\sqrt{S_I(f = 50\,\mathrm{MHz})} = \sqrt{2e\,\langle I\rangle}$, $\langle I\rangle$ denoting the time-averaged photocurrent, while the technical-noise contribution arises from fluctuations in the expected photocurrent $I(t)$ and scales linearly with the detected photocurrent. We observe that downsampling by a factor of four leads to a multiplication of the amplitude of the technical noise by a factor of ∼1.7 on the optical signal relative to the carrier, which due to finite noise bandwidth is somewhat less than the factor of two (four, in electrical power units) which would be expected for ideal downsampling by a factor of four in the presence of white technical noise. These results further demonstrate that, properly implemented, downsampling does not magnify noise on the pulse train to a degree which is prohibitive for applications.
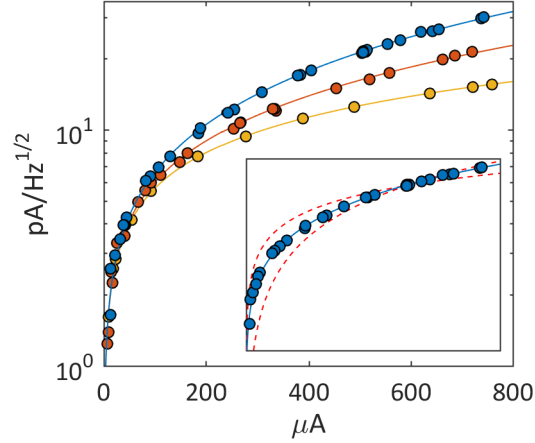

Figure 3.4: **Effect of downsampling on photocurrent fluctuations.** Fluctuations at 50 MHz Fourier frequency in the detected photocurrent as a function of the time-averaged photocurrent in three cases: CW laser at the shot-noise limit (lowest, yellow), 10 GHz pulse train (middle, red), and 2.5 GHz down-sampled pulse train (highest, blue). Dots show measured data and curves show fits to the data. The fit for the shot-noise-limited laser has a single free parameter, which is a scaling factor of order 1 due to frequency dependence of the photo-detector's trans-impedance gain. The fits for the pulse trains have a scaling factor in common, and have as an additional parameter the amplitude of the technical noise on the pulse train. This is -153.9 dBc/Hz for the 10 GHz pulse train and increases by a factor of ∼1.72 to -149.3 dBc/Hz for the 2.5 GHz downsampled pulse train. Inset: Optimized fits (dashed red) to the experimental data for the downsampled 2.5 GHz pulse train using only shot-noise or linear technical noise scaling, demonstrating that both noise processes are important for explaining the data.

3.4.1 Model for the effect of incomplete extinction of rejected pulses and amplification of a downsampled pulse train

To this point, we have considered effects of downsampling assuming that extinction of the rejected pulses is complete, but in a practical application this is not necessarily the case. The modulators used for pulse extinction may transmit a substantial amount of energy from the rejected pulses—for example, one commercial manufacturer specifies 25 dB extinction ratio, this number vary in practice. Additionally, the electronic gating signal may not have sufficient bandwidth to completely switch from transmission to extinction within the repetition period of the incoming pulse train, and initial extinction can be followed by some transmission caused by ringing in the gating signal. Bandwidth limitations will be increasingly likely as the repetition rates of frequency combs increase, placing more demanding requirements on gating electronics. Incomplete extinction will add modulations to the optical spectrum and will raise the total power of the downsampled pulse train while keeping the energy of the fully-transmitted pulses fixed. This will require higher average power to achieve a given target pulse energy.

The effects of incomplete extinction of rejected pulses are exacerbated if the incomplete extinction does not happen in a deterministic and repetitive fashion; this could occur, for example, if intermediate pulses fall near the edge of the gate in the presence of relative timing jitter between the optical and electronic pulse trains; or if the extinction ratio fluctuates in time. Interestingly, if the downsampled pulse train is subsequently amplified and spectrally broadened, the impact of incomplete extinction depends on whether the optical amplifier used operates in the linear regime or in the saturated regime.

As an example, we consider the case where each fully transmitted pulse is preceded and followed by partially-extinguished pulses whose amplitudes fluctuate for each period of the downsampled pulse train. This fluctuation could occur because the pulses lie on the edge of the electronic gate and there is relative timing jitter between the optical pulse train and the gating signal. It is true that these fluctuations will lead to decoherence during nonlinear spectral broadening. However, the coherence is

degraded by this mechanism only within the bandwidth that is achieved by the broadened, partially-extinguished pulses. In efficient $f - 2f$ interferometry only the fully-transmitted pulses should reach an octave in bandwidth. Therefore, this mechanism of supercontinuum decoherence is not a problem in $f - 2f$ interferometry in general, unless there is coupling between the amplitudes of the amplified partially-extinguished pulses and the amplified fully transmitted pulses. This coupling can arise, for example, through amplification in the saturation regime, which then leads to decoherence across the full bandwidth of the supercontinuum.

To illustrate this point, we have performed numerical simulations of the spectral broadening of a 100 GHz train of 100 fs pulses which has been downsampled to 10 GHz and then amplified. We use an adaptive[14] split-step Fourier method[15] to simulate spectral broadening in 30 cm of HNLF according to the generalized nonlinear Schrodinger equation[16] (see Appendix **??**. In the simulation each fully-transmitted pulse, amplified to 1 nJ, is preceded and followed by partially-extinguished pulses with normally distributed and uncorrelated energies with mean of 0.3 nJ and standard deviation of 0.225 nJ. This models the effect of adjacent pulses which coincide with the edge of the gate. We simulate amplification in two regimes: saturation is simulated using a fixed-energy method wherein the pulse energies in each three-pulse burst are re-scaled by a common factor so that the total energy is 1.6 nJ; linear amplification is simulated using a fixed-gain model, which involves no such rescaling of pulses. Numerically, we simulate the spectral broadening of each pulse individually, which is acceptable because terms in the generalized non-linear Schrodinger equation operate only locally or, in the case of the Raman term, on the timescale of several femtoseconds, while the separation between the pulses in each burst is 10 ps (the inverse of the initial 100 GHz repetition rate). We have verified that during simulated time-evolution each broadened pulse remains well-centered in its 5 ps simulation window.

Results of this study are shown in Figure 3.5. Figure 3.5a depicts a three-pulse burst before and after propagation in HNLF. In Figure 3.5b we show spectra corresponding to spectral broadening of this three-pulse burst, as well as plots of the spectral coherence averaged over many simulations.

The first-order spectral coherence $g_{12}^{(1)}(\lambda)$ is defined as:

$$\left| g_{12}^{(1)}(\lambda) \right| = \left| \frac{\langle E_1^*(\lambda) E_2(\lambda) \rangle}{\sqrt{\langle |E_1(\lambda)|^2 \rangle \langle |E_2(\lambda)|^2 \rangle}} \right| = \left| \frac{\langle E_1^*(\lambda) E_2(\lambda) \rangle}{\langle |E(\lambda)|^2 \rangle} \right|. \tag{3.5}$$

Curves are plotted for the fixed-gain and fixed-energy cases, as well as for the case with ideal downsampling (no partially-extinguished pulses) and only shot-noise on the pulse train. The averages in the formula above are over 1000 instantiations of the pair E_1 and E_2, for a total of 2000 broadened spectra for each pulse within the burst of three. In both the fixed-gain and fixed-energy cases the coherence is poor in the center of the spectrum, but in the fixed-gain case, which models amplification in the linear regime, the coherence is preserved in the high- and low-frequency ends of the spectrum where it is needed for self-referencing.
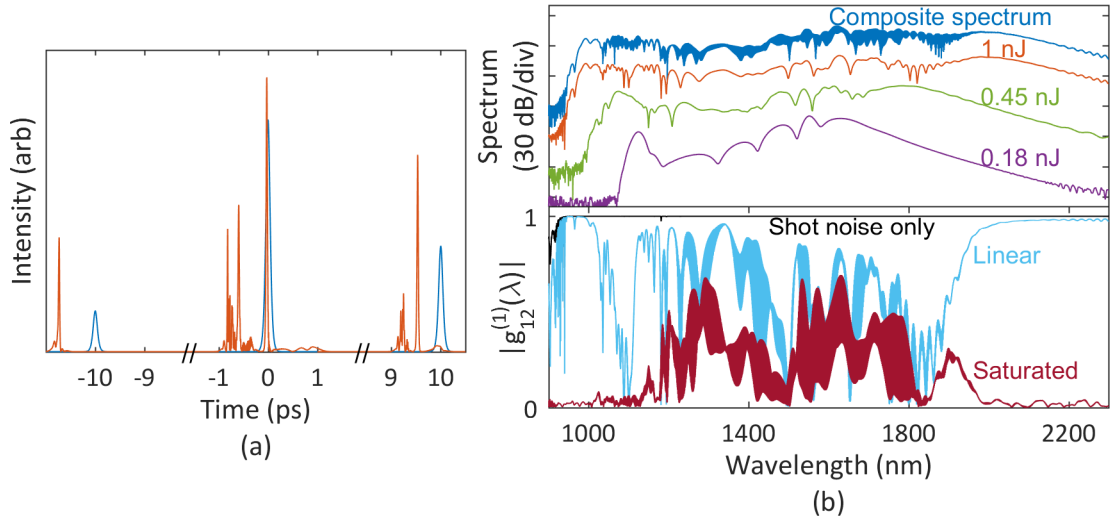

Figure 3.5: **Investigation of incomplete pulse extinction and amplification.** Investigation of incomplete pulse extinction and amplification. (a) A burst consisting of a fully-transmitted 1 nJ, 100 fs pulse and 100 fs partially-transmitted adjacent pulses with energies of 0.18 nJ and 0.45 nJ. Blue indicates initial sech^2 pulses, and orange indicates the intensity after propagation through 30 cm HNLF. Note that the x-axis has been broken. (b) Top panel: optical spectra corresponding to the pulses shown in orange in (a), showing the composite spectrum of the three pulses (top, blue) and the spectra of the 1 nJ central pulse (second, orange), the 0.45 nJ adjacent pulse (third, green), and the 0.18 nJ adjacent pulse (bottom, purple). Bottom panel: Calculated spectral coherence averaged over 2000 simulations for the case of shot-noise only (top, black) and for the case of fluctuating amplitudes of the first and last pulses as described in the text, after simulated amplification in a linear-regime optical amplifier (second, teal), and a saturated optical amplifier (bottom, maroon). For the case of linear-regime operation, high spectral coherence is preserved in the extreme ends of the supercontinuum even as it is lost in the center, in contrast with the complete loss of coherence after amplification in saturation.

3.4.2   Further remarks on the application of downsampling

Downsampling via pulse gating is a promising tool to manipulate high-repetition-rate frequency combs from low size, weight, and power packages and to aid in the detection of their offset frequencies. In our experiments downsampling enabled detection of f_0 at a signal-to-noise ratio sufficient for measurement and stabilization, which otherwise would have required significantly higher average power. The effects of the electronic timing jitter of the gate signal are negligible so long as incoming optical pulses do not arrive coincidentally with the edge of the gate; when they do, timing jitter induces amplitude noise on the transmitted pulses. This results in an increase in RMS optical pulse energy fluctuations σ_{PEF}. Independently, the PSD of pulse energy fluctuations may be increased by aliasing of technical noise and by shot noise, depending on the relative magnitudes of these two types of noise. Each of these sources of signal-to-noise-ratio degradation has the potential to interfere with detection of f_0. This investigation of these challenges will facilitate application of the technique in high-repetition-rate frequency comb systems. Importantly, our experiments demonstrated that downsampling does not add a significant amount of noise to the frequency components of the pulse train, and in a separate experiment the technique has recently been used successfully to detect the carrier-envelope offset frequency of a 10 GHz comb by downsampling by a factor of four[4].

To employ downsampling as demonstrated here with repetition rates >10 GHz will require electronic gates with duration ≤100 ps. Technology to downsample with gates as short as 20 ps is commercially available, while 100 Gb/s integrated circuits and 25 GHz demultiplexing have been demonstrated[17, 18]. Barring the use of such state-of-the-art electronics, pulse gates of duration longer than the incoming optical pulse train's repetition period can be employed. This will be technically easier to achieve, but will result in additional modulations on the spectrum of the downsampled pulse train.

The ambiguity of the input comb's offset frequency as a result of the reduction of the offset frequency modulo the new repetition rate makes downsampling most suitable for applications where the ambiguity can be removed by some other method. Two such applications are frequency comb

calibration of astronomical spectrographs, where measurement of the wavelength of a comb mode can remove the ambiguity, and microresonator-based frequency combs, where the uncertainty in the offset frequency is determined by the frequency stability of the pump laser and can be much less than the repetition rate of the downsampled comb.

References

[1]   A. Turing. The Chemical Basis of Morphogenesis. *Philosophical Transactions of the Royal Society B*, 237, **1952**, 37–72 (cited on page 1).

[2]   A. J. Metcalf, V. Torres-company, D. E. Leaird, S. Member, A. M. Weiner, and A. Broadband. High-Power Broadly Tunable Electrooptic Frequency Comb Generator. *IEEE Journal of Selected Topics in Quantum Electronics*, 19 (6), **2013**, 3500306. URL: `http://ieeexplore.ieee.org/stamp/stamp.jsp?arnumber=06553388` (cited on page 3).

[3]   A. M. Weiner. Femtosecond pulse shaping using spatial light modulators. *Review of Scientific Instruments*, 71 (5), **2000**, 1929–1960. DOI: `10.1063/1.1150614` (cited on page 6).

[4]   K. Beha, D. C. Cole, P. Del'Haye, A. Coillet, S. A. Diddams, and S. B. Papp. Electronic synthesis of light. *Optica*, 4 (4), **2017**, 406–411. DOI: `10.1364/OPTICA.4.000406` (cited on pages 6, 9, 24).

[5]   a. a. Amorim, M. V. Tognetti, P Oliveira, J. L. Silva, L. M. Bernardo, F. X. Kärtner, and H. M. Crespo. Sub-two-cycle pulses by soliton self-compression in highly nonlinear photonic crystal fibers. *Optics letters*, 34 (24), **2009**, 3851–3853. DOI: `10.1364/OL.34.003851` (cited on page 7).

[6]   S. Backus, C. G. Durfee, M. M. Murnane, and H. C. Kapteyn. High power ultrafast lasers. *Review of Scientific Instruments*, 69 (3), **1998**, 1207. DOI: `10.1063/1.1148795` (cited on page 11).

[7]   A. Baltuska, M. Uiberacker, E. Goulielmakis, R. Kienberger, V. S. Yakovlev, T. Udem, T. W. Hänsch, and F. Krausz. Phase-Controlled Amplification of Few-Cycle Laser Pulses. *IEEE Journal of Selected Topics in Quantum Electronics*, 9 (4), **2003**, 972–989 (cited on page 11).

[8]   C. Gohle, J. Rauschenberger, T. Fuji, T. Udem, A. Apolonski, F. Krausz, and T. W. Hänsch. Carrier envelope phase noise in stabilized amplifier systems. 30 (18), **2005**, 2487–2489 (cited on pages 11, 18).

[9]   J. Rauschenberger, T. Fuji, M. Hentschel, A.-J. Verhoef, T. Udem, C. Gohle, T. W. Hänsch, and F. Krausz. Carrier-envelope phase-stabilized amplifier system. *Laser Physics Letters*, 3 (1), **2006**, 37–42. DOI: `10.1002/lapl.200510053` (cited on page 11).

[10] M. Hirano, T. Nakanishi, T. Okuno, and M. Onishi. Silica-Based Highly Nonlinear Fibers and Their Application. *Sel. Top. Quantum Electron.*, 15 (1), **2009**, 103–113. DOI: `10.1109/JSTQE.2008.2010241` (cited on page 13).

[11]   D. Mandridis, I. Ozdur, F. Quinlan, M. Akbulut, J. J. Plant, P. W. Juodawlkis, and P. J. Delfyett. Low-noise, low repetition rate, semiconductor-based mode-locked laser source suitable for high bandwidth photonic analog – digital conversion. *Applied Optics*, 49 (15), **2010**, 2850–2857 (cited on page 15).

[12]   J. M. Dudley, G. G. Genty, and S. Coen. Supercontinuum generation in photonic crystal fiber. *Reviews of Modern Physics*, 78 (4), **2006**, 1135–1184. DOI: `10.1103/RevModPhys.78.1135` (cited on page 16).

[13]   D. C. Cole, K. M. Beha, S. A. Diddams, and S. B. Papp. Octave-spanning supercontinuum generation via microwave frequency multiplication. *Proceedings of the 8th Sympsion on Frequency Standards and Metrology 2015, Journal of Physics: Conference Series*, 723, **2016**, 012035. DOI: `10.1088/1742-6596/723/1/012035` (cited on page 19).

[14]   A. M. Heidt. Efficient Adaptive Step Size Method for the Simulation of Supercontinuum Generation in Optical Fibers. *Journal of Lightwave Technology*, 27 (18), **2009**, 3984–3991 (cited on page 22).

[15]   J. Hult. A Fourth-Order Runge-Kutta in the Interaction Picture Method for Simulating Supercontinuum Generation in Optical Fibers. *Journal of Lightwave Technology*, 25 (12), **2007**, 3770–3775. DOI: `10.1109/JLT.2007.909373` (cited on page 22).

[16]   G. P. Agrawal. **Nonlinear Fiber Optics**. 4th. Burlington, MA: Elsevier, 2007 (cited on page 22).

[17]   R. Driad, J. Rosenzweig, R. E. Makon, R. Lösch, V. Hurm, H. Walcher, and M. Schlechtweg. InP DHBT-Based IC Technology for 100-Gb / s Ethernet. *IEEE Trans. on Electron. Devices*, 58 (8), **2011**, 2604–2609 (cited on page 24).

[18]   D. Ferenci, M. Grozing, M. Berroth, R. Makon, R. Driad, and J. Rosenzweig. A 25 GHz Analog Demultiplexer with a Novel Track and Hold Circuit for a 50 GS / s A / D-Conversion System in InP DHBT Technology. In: **Microwave Symposium Digest**. 2012, pp. 1–3 (cited on page 24).